

Application of Berendsen barostat in dissipative particle dynamics for nonequilibrium dynamic simulation

Yuqing Lin,^{a)} Dingyi Pan,^{b)} Jiaming Li, Lingxin Zhang, and Xueming Shao

State Key Laboratory of Fluid Power and Mechatronic Systems, Key Laboratory of Soft Machines and Smart Devices of Zhejiang Province, Department of Engineering Mechanics, Zhejiang University, Hangzhou 310027, China

(Received 21 November 2016; accepted 7 March 2017; published online 23 March 2017)

The Berendsen barostat from molecular dynamics simulation is applied in both standard dissipative particle dynamics (DPD) and many-body dissipative particle dynamics (MDPD) simulations. The original Berendsen barostat works well in (M)DPD simulation of a single-component system under constant pressure condition and in nonequilibrium dynamic processes. The partial Berendsen barostat is proposed for multi-component system simulation with (M)DPD. The displacement rescaling process of the Berendsen barostat is only applied on the particles outside the center region, acting as a pressure “boundary condition.” The center part forms the free zone, in which the interface shape and nonequilibrium dynamic behavior between different phases can be captured properly. An immiscible bubble in the second fluid under constant pressure condition is studied, and the oscillation of the bubble radius and fluctuation of system pressure can be obtained by the current barostat. Preliminary models for bubble growing and collapsing under square pressure wave and bubble oscillation under harmonic pressure wave are also reported in the current simulation. It shows that the partial Berendsen barostat is suitable for the modeling of nonequilibrium process of single or few droplets/bubbles in multi-component systems. *Published by AIP Publishing.* [<http://dx.doi.org/10.1063/1.4978807>]

I. INTRODUCTION

Particle-based mesoscale modeling techniques have become promising and important tools for simulations of polymeric or colloidal fluid, blood flow, nanoparticle across membrane, and other complex fluid systems, whose crucial scales are typically in 10–100 nm and 1 ns–10 ms.^{1,2} These methods possess the unique ability to model relatively large physical systems, and at the same time, effectively capture the essential features of the micro- and nanoscale structures, architectures, and relevant interactions.¹ Comparing with microscopic approaches, the mesoscopic methods can access large systems at a lower computational cost. Meanwhile, the continuum description becomes challenging in modeling hydrodynamics at microscopic and mesoscopic scales because of the intrinsic structures and microscale behaviors of fluids. With these characteristics, the mesoscale model could be a suitable medium between micro- and macroscopic modeling methods.

It is a very popular way to construct a mesoscale model via coarse-graining (CG) procedures, which drastically simplify the atomistic dynamics by using a CG particle to represent a cluster of molecules. Dissipative particle dynamics (DPD) is one of them and has been applied successfully in the study on various systems, for example, colloidal suspensions,^{3,4} polymer solutions,^{5–10} two-phase flow,^{11–14} surfactants,^{15–18} biological membranes,^{19–23} and drug delivery.^{24–28} However, the original DPD method owns its limitation that its

inter-particle force, i.e., conservative interaction, leads to an ideal fluid system. In order to approach the real fluid system, the many-body dissipative particle dynamics (MDPD) method is proposed. After adding a density dependent interaction part into the conservative force, the van der Waals loop can be included in MDPD.

The interest of studying property as a function of temperatures and pressures is much more extensive than the interest of using volume and energy as the independent variables.²⁹ In fact, temperature and pressure are quantities which are typically constant in experiments. In (M)DPD, a natural thermostat has been already incorporated.² Therefore, the barostat for pressure control could be a very important part for the (M)DPD application. As we known, the constant-pressure is highly common in theories, numerical simulations, and experiments. Therefore, it is necessary to build the practicable barostat for (M)DPD.

As a CG method originating from molecular dynamics (MD), (M)DPD usually borrows the barostat models from MD. Trofimov *et al.*² applied the Andersen barostat to produce the *NPT* ensemble in (M)DPD. Using Shardlow-like splitting algorithms, Lísal *et al.*³⁰ achieved the isobaric conditions in DPD. The Langevin piston approach was applied in DPD to obtain the constant pressure condition.³¹ The DL_MESO_DPD code included the Berendsen barostat²⁹ into its barostat group.³² Moreover, Atashafrooz and Mehdipour³³ applied MDPD coupling with the Berendsen barostat to simulate liquid-vapor coexistence of sodium, and their MDPD results were more accurate than those obtained by pair potentials and potential of mean force. The above work proved that the barostat from MD can be successfully applied in (M)DPD.

^{a)}Electronic mail: linyuqing@zju.edu.cn.

^{b)}Author to whom correspondence should be addressed. Electronic mail: dpan@zju.edu.cn

However, to the knowledge of authors, the nonequilibrium dynamic simulation coupling with pressure control in (M)DPD has not been reported or investigated.

Specifically, the Berendsen barostat uses an external bath to make global pressure weakly coupled to a pressure bath, which can be easily applied to the existing program without major modification, and it is ideally suited to nonequilibrium molecular dynamics (NEMD).²⁹ The original Berendsen barostat could be a good barostat for (M)DPD simulation in a single-component system. However, for application in multi-component system and nonequilibrium dynamic processes, the rescaling of particle displacement will bring unphysical influence to the interface formation, and it is not able to capture correct nonequilibrium dynamic behaviors. In this paper, we propose the partial Berendsen barostat by shifting the rescaling area far away from the interface to reduce this unphysical influence and, meanwhile, retain its advantage in nonequilibrium dynamic simulation. In the following, the general theory of (M)DPD is given in Sec. II, followed by the detailed introduction of the original Berendsen barostat and application in a single-component system. In Sec. IV, the partial Berendsen barostat and its application in the multi-component system are presented. The conclusion is drawn in Section V.

II. GENERAL THEORY

A. Method introduction

The standard version of the DPD method was first introduced by Hoogerbrugge and Koelman³⁴ in 1992 and was considered as one of the CG approaches of MD simulation. The MDPD method is the development of the standard DPD aiming to construct a nonideal fluid system. In standard DPD, the forces depend linearly on the inter-particle separation, and the DPD fluid is not able to exhibit liquid–vapor phase coexistence and transition. To overcome this, the MDPD method, first introduced by Pagonabarraga and Frenkel³⁵ and improved by Trofimov *et al.*,³⁶ adopts a density depended part adding into the conservative force. Overall, the motion of each (M)DPD particle is governed by Newton's second law,

$$\mathbf{v}_i = \frac{d\mathbf{r}_i}{dt}, \quad \mathbf{f}_i = \frac{d\mathbf{v}_i}{dt}, \quad (1)$$

where \mathbf{r}_i and \mathbf{v}_i are the position and velocity vectors of particle i . \mathbf{f}_i is the summation of inter-particle forces exerted by all the other particles. Español and Warren³⁷ suggested that the inter-particle force \mathbf{f}_i can be decomposed by three pairwise and center-to-center forces, i.e., conservative force, dissipative force, and random force,

$$\mathbf{f}_i = \sum_{j \neq i} (\mathbf{F}_{ij}^C + \mathbf{F}_{ij}^D + \mathbf{F}_{ij}^R). \quad (2)$$

The dissipative and random forces can be calculated as follows:

$$\begin{aligned} \mathbf{F}_{ij}^D &= -\gamma w^D(r_{ij}) \hat{\mathbf{r}}_{ij} \cdot \mathbf{V}_{ij} \hat{\mathbf{r}}_{ij}, \\ \mathbf{F}_{ij}^R &= \sigma w^R(r_{ij}) \theta_{ij} \hat{\mathbf{r}}_{ij}, \end{aligned} \quad (3)$$

where γ and σ are the amplitudes of dissipative and random forces, respectively. \mathbf{r}_{ij} and \mathbf{V}_{ij} are relative distance and velocity of particle i and particle j . We also have $r_{ij} = |\mathbf{r}_{ij}|$ and $\hat{\mathbf{r}}_{ij} = \mathbf{r}_{ij}/r_{ij}$. θ_{ij} is a randomly fluctuating variable with Gaussian

statistics which satisfies $\langle \theta_{ij} \rangle = 0$ and $\langle \theta_{ij}(t)\theta_{kl}(t') \rangle = (\delta_{ik}\delta_{jl} + \delta_{il}\delta_{jk})\delta(t - t')$. w^D and w^R are the weight functions of the dissipative and random forces, which are short-ranged so that all these forces vanish for $r_{ij} \geq r_c$. The random force weight function is given by

$$w^R(r_{ij}) = \begin{cases} 1 - \frac{r_{ij}}{r_c}, & r_{ij} < r_c, \\ 0, & r_{ij} \geq r_c. \end{cases} \quad (4)$$

According to Español and Warren,³⁷ coefficients and weight functions in Eq. (3) should follow certain constraints to fulfill the fluctuation–dissipation theorem. In detail, if one of the coefficients and weight functions are chosen arbitrarily and then the others should be determined by

$$w^D(r_{ij}) = [w^R(r_{ij})]^2, \quad \text{and} \quad \sigma^2 = 2\gamma k_B T, \quad (5)$$

where $k_B T$ is the Boltzmann temperature of the system.

For the conservative force, in DPD, it is given by

$$\mathbf{F}_{ij}^C = a_{ij} w^C(r_{ij}) \hat{\mathbf{r}}_{ij}, \quad (6)$$

where a_{ij} is the conservative coefficient, and we choose $w^C(r_{ij}) = w^R(r_{ij})$. In MDPD, Warren¹¹ proposed the conservative force for the vapor–liquid coexistence system in the van der Waals fluid, its expression is given by

$$\mathbf{F}_{ij}^C = [A_{ij} w_C(r_{ij}) + B_{ij}(\bar{\rho}_i + \bar{\rho}_j) w_d(r_{ij})] \hat{\mathbf{r}}_{ij}. \quad (7)$$

This conservative force consists of two parts: a density-independent attractive force ($A_{ij} < 0$), which is similar to DPD conservative force, and a repulsive force ($B_{ij} > 0$) depending on the instantaneous local particle density, i.e., a many-body interaction.³⁶ $\bar{\rho}_i$ and $\bar{\rho}_j$ are the local instantaneous densities on the position of particle i and j . Similarly, the weight function adopts the same formula as standard DPD, but the two parts conservative force have different cutoff distances, r_c and r_d , for weight functions, w_C and w_d , respectively. The dissipative and random force is kept the same as those of standard DPD, and their cut-off distance is r_c .

The definition of the instantaneous local density is

$$\bar{\rho}_i = \sum_{j \neq i} \frac{15}{2\pi r_d^3} w_\rho(r_{ij}), \quad (8)$$

and the identical formula of the weight function from Eq. (4) is used to construct w_ρ by $r_c = r_d$, which makes it to be normalized as

$$\frac{15}{2\pi r_d^3} \int_0^\infty w_\rho(r) d^3 r = 1. \quad (9)$$

In our simulation, particles are initially located at the sites of face centers and apexes of cubic lattices. Meanwhile, the initial velocities of all particles are set randomly according to the initial system Boltzmann temperature, $k_B T$. A modified version of the velocity–Verlet algorithm^{38,39} is used to advance the particle position and velocity. In this paper, the DPD parameters for different cases are chosen the same as in Table I, if it is not indicated specifically. Here, L_0 is the initial side length of the computation cube, N is the particle number, Δt is the time step, and λ is an empirical parameter for the velocity–Verlet algorithm. We control the pressure by the barostat when the time (t) is t_J and we define $t^* = t - t_J$.

TABLE I. Parameters in the current (M)DPD simulations.

L_0	N	Δt	$k_B T$	γ	λ	t_J
26.2	108 000	0.01	1.0	4.5	0.65	200

B. Equation of state (EOS)

The standard DPD, as a successful mesoscale method to mimic hydrodynamics, is not flexible enough to simulate the accurate thermodynamic behavior of a real system. The most substantial reason is that its conservative force produces equation of state (EOS) which is different from the real fluid. There is an approximate DPD fluid EOS given by the following equation:³⁹

$$P = \rho k_B T + \alpha a \rho^2 \quad (\alpha = 0.101 \pm 0.001), \quad (10)$$

where P and ρ are the pressure and the number density of the DPD particles, a is the repulsive strength which is equal to a_{ij} for all particle pairs in a single-component system, and α is a fitting parameter. For $\rho \geq 2$ and $a \geq 15$, it is a good approximation verified by Groot and Warren.³⁹ This DPD EOS has a rigid quadratic density dependence irrespective of the parameter values.³⁹

Comparing with the standard DPD, the MDPD method adopts a different definition of the conservative force. For the vapor–liquid system, the MDPD conservative force, Eq. (7), produces a different EOS. After a series of simulations, Warren¹¹ gave its fitting equation as

$$P = \rho k_B T + \alpha A \rho^2 + 2\alpha B r_d^4 (\rho^3 - c \rho^2 + d), \quad (11)$$

where $A(<0)$ and $B(>0)$ are the attractive and repulsive strengths (for a single-component system, $A_{ij} = A$ and $B_{ij} = B$ for all particle pairs); α , c , and d are the fitting parameters, which are equal to 0.101 ± 0.001 , 4.16 ± 0.02 , and 18 ± 1 , respectively. r_d is the cut-off distance of a repulsive part. For $\rho \geq 5$ and $-A \approx B \approx 30$, Eq. (11) is a good approximation shown by Warren.¹¹ The EOS contains a van der Waals loop which is able to construct the vapor–liquid coexistence. The phase separation is found in a range of densities $\rho_V < \rho < \rho_L$, where ρ_V and ρ_L are the vapor and liquid densities, respectively.

In order to find a reliable range of densities (pressure), in which these EOSs are valid in the current simulation, we first run several validation cases. The simulation system contains 8000 particles in a cubic box. The repulsive parameter is $a_{ij} = B_{ij} = 25$ for DPD and MDPD, respectively, and the attractive parameter is $A_{ij} = -40$ for MDPD. The pressure is obtained by averaging the stress tensor trace,⁴⁰ and the lattice stress tensor is calculated through the virial process⁴¹

$$\mathbf{S}_{\alpha\beta} = -\frac{1}{V} \left(\sum_i^{N_p} m u_{i\alpha} u_{i\beta} + \sum_i^{N_p} \sum_{j>i}^{N_p} r_{ij\alpha} F_{ij\beta} \right), \quad (12)$$

where V is the volume of the lattice, N_p is the number of particles in the lattice, m is the mass of particle i , $u_{i\alpha}$ and $u_{i\beta}$ are the fluctuating velocity components of particle i , defined by $u_{i\alpha} = v_{i\alpha} - \bar{v}_\alpha(\mathbf{r})$ ($v_{i\alpha}$ is the velocity component of particle i and \bar{v}_α is the stream velocity at position \mathbf{r}), $r_{ij\alpha}$ and $F_{ij\beta}$ are the inter-distance and inter-force components between the

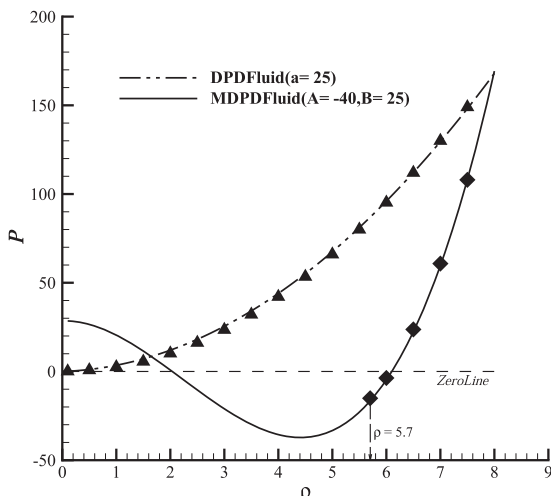


FIG. 1. Simulating results of EOSs of (M)DPD. The dashed line (*Zeroline*) represents zero pressure ($P = 0$).

particles i and j , and the angular bracket $\langle \dots \rangle$ means an ensemble average.

The results are shown in Fig. 1, which largely agree with Eqs. (10) and (11). In our results, there are some differences compared with the previous work.^{11,39} In the result of MDPD EOS, the vapor–liquid heterogeneous region will occur when the initial density is less than 5.7 in our *NVT* ensemble simulation, where the vapor region means the no-particle region.

III. SINGLE-COMPONENT SYSTEM

A. Berendsen barostat

The Berendsen barostat proposes an external bath so that the global pressure is weakly coupled to this “pressure bath” and the volume is periodically rescaled, using the principle of the least local perturbation consistent with the required global coupling. Since the coupling strength can be varied, the effect of coupling can be easily evaluated and controlled.²⁹

Consider a cubic system which contains N molecules and its volume is $V = L^3$. The Berendsen barostat uses a scale factor, μ , which is a function of pressure, P , to scale lengths of the system,

$$\mathbf{r}_i \rightarrow \mu \mathbf{r}_i \quad (i = 1, 2, \dots, N) \quad \text{and} \quad L \rightarrow \mu L, \quad (13)$$

where \mathbf{r}_i is the position of the i th molecule. μ is given by

$$\mu = \left[1 - \frac{\Delta t}{\tau_P} (P - P_0) \right]^{1/3}. \quad (14)$$

Here, Δt is the time step, τ_P is the “rise time” of the barostat, and P_0 is the desired pressure. After the scaling process through Eq. (13), the system volume becomes $V = (\mu L)^3 = [1 - \frac{\Delta t}{\tau_P} (P - P_0)] V_0$ and each molecule position vector turns to be $\mu \mathbf{r}$. This rescaling process is easy to implement for programming.

B. Application in (M)DPD simulation

The original Berendsen barostat is applied to the single-component system of (M)DPD simulation, and the relevant

TABLE II. Parameters in (M)DPD simulations of the single-component system.

	A_{ij}/a_{ij}	B_{ij}	r_C	r_d	P_0
DPD	25	/	1.0	/	150
MDPD	-40	25	1.0	0.75	50

parameters are given in Table II. An alternative approach of pressure calculation is also used in the following, i.e., the local pressure can be obtained from EOSs by calculating the instant particle number density. The results are shown in Fig. 2, and the results demonstrate that the original Berendsen barostat could be a good barostat to control pressure in (M)DPD. Besides, due to the (M)DPD natural thermostat, the temperature is kept at a steady value, except the period of drastic pressure rising.

The effect of τ_P is also presented in Fig. 2, with τ_P in the value of 10, 100, and 1000. It shows that all the pressure magnitudes ascend to the desired pressure (P_0). The larger τ_P , the longer time the system takes to reach P_0 . We also find that the natural thermostat of (M)DPD works well to recover the system temperature to the preset value after the adiabatic heating. It is worthy to mention that the steady system temperature is a little lower than its preset value, $k_B T = 1$, with a relative error less than 1%. This deviation is determined by the selection of numerical time step and empirical parameter λ .^{39,42}

In addition, the isothermal compressibility is also calculated from the system volume fluctuation under the *NPT* ensemble,³⁸ and the results are shown in Table III. The

TABLE III. Effect of τ_P on fluid isothermal compressibility (κ_T).

τ_P	κ_T (DPD)	κ_T (MDPD)
10	2.65×10^{-3}	4.57×10^{-3}
100	0.96×10^{-3}	2.76×10^{-3}
1000	0.05×10^{-3}	0.41×10^{-3}

isothermal compressibility changes significantly with the variation of τ_P , indicating that the incorporated barostat changes the properties of the system. Furthermore, the dimensionless compressibility can be derived from this isothermal compressibility,³⁹ and current simulations show that $\tau_P = 10$ in DPD and $\tau_P = 10 \sim 100$ in MDPD can reproduce the dimensionless compressibility in the same order of magnitude with the one of water, which would be the suitable values for simulating water.

C. Nonequilibrium dynamics in single-component system

In the results of Subsection III B, the fluid pressure rises quickly under the control of the Berendsen barostat. With $\tau_P = 10$, the system just takes about 20 steps to jump to the desired pressure, corresponding to the rising time equal to 0.2. In the following, we use two kinds of wave functions of pressure control, i.e., square wave and harmonic wave, to demonstrate this characteristic in MDPD simulation. These two wave functions are given by

$$P_0^* = P_0 - P_a(-1)^{[2f \cdot t^*]}, \quad (15)$$

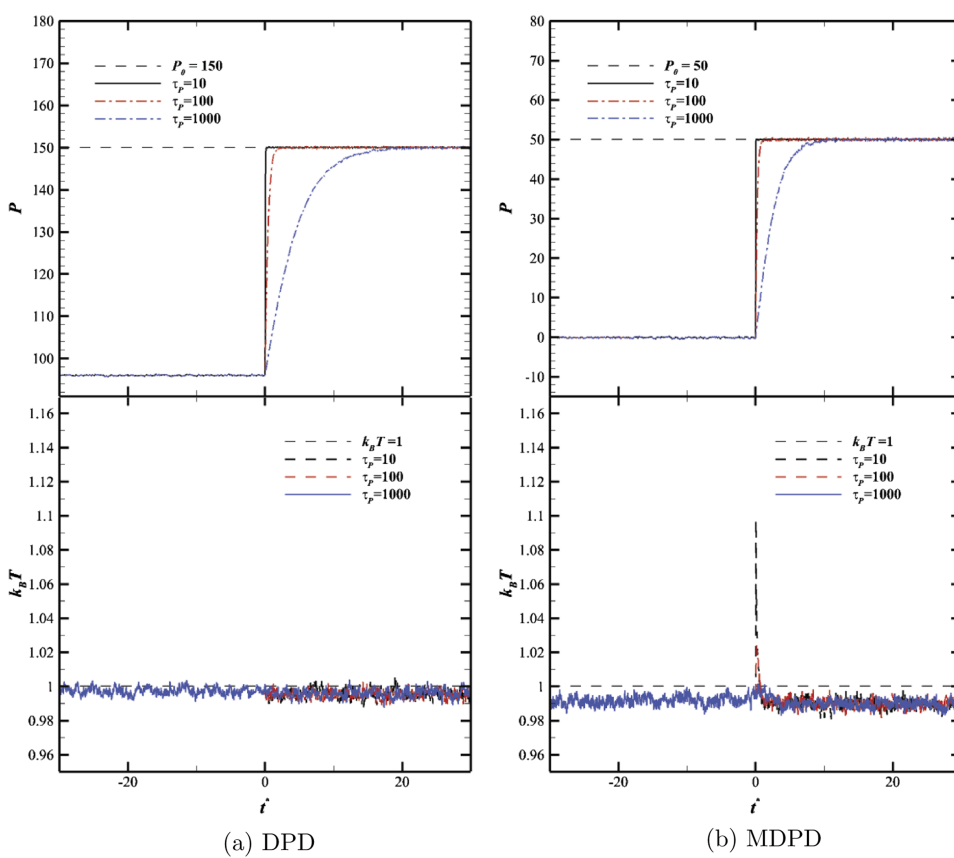


FIG. 2. (M)DPD simulations at constant pressure condition by the Berendsen barostat in the single-component system.

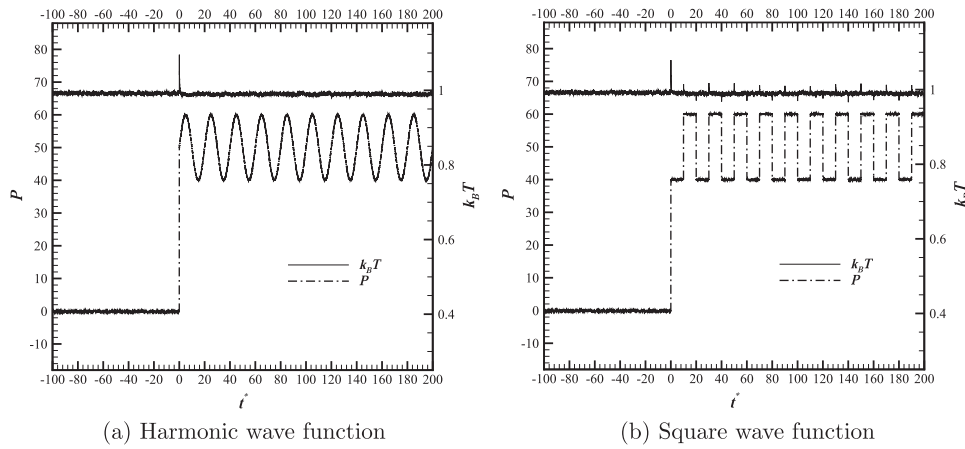


FIG. 3. MDPD simulation in the single-component system under wave pressure conditions by the Berendsen barostat ($\tau_P = 10$).

$$P_0^* = P_0 + P_a \sin(2\pi f \cdot t^*), \quad (16)$$

where P_0 is the original pressure shown in Table II, and P_0^* is the desired pressure, and P_a and f are the amplitude and frequency of wave, respectively. In addition, $[\dots]$ denotes the floor function. Eq. (15) represents the square wave function, and Eq. (16) is the harmonic wave function.

We set $P_a = 10$ and $f = 0.05$ in the current simulation. The results are shown in Fig. 3, and the instantaneous pressure values agree very well with our desired pressure wave shape (P_0^*). Comparing two kinds of waves, we can see that the natural thermostat will lead to the adiabatic heating when the pressure changes drastically at the early stage. On the contrary, it will not lead to adiabatic heating when pressure changes steadily and gradually, even if τ_P is small.

IV. PARTIAL BERENDSEN BAROSTAT FOR MULTI-COMPONENT SYSTEM

A. Partial Berendsen barostat

Concerning the study on the multi-component system, on one hand, the constant pressure condition or pressure control is also meaningful and useful, which is common in experimental studies.² On the other hand, the internal dynamic behaviors between different phases are important; in other words, the nonequilibrium dynamic process (NEDP) should be captured properly. For example, bubble (gaseous phase) collapses in the liquid phase may cause a significant pressure pulse and propagate outward,⁴³ and also the bubble shape or phase interface is fully determined by its surrounding fluid environment. However, in the constant pressure application in the single-component system as mentioned above, the Berendsen barostat requires two rescaling processes, applying on the computation region size and the displacement of all the particles, respectively. The rescaling processes applying on all the particles could cause an artificial effect on the multi-component system, which is not expected in multi-component modeling. To overcome this, the partial Berendsen barostat is proposed in this section.

In general, the partial Berendsen barostat only applies the displacement rescaling process to a part of the particles in the domain, which is far away from the places where we are curious of the multi-component dynamic behavior. In this situation, the partial Berendsen barostat acts as a constant

pressure “boundary condition” of the domain. The schematic is shown in Fig. 4. For simplification, the region division between the free zone and rescaling zone in only one direction is shown in this figure. We bring a new variable which accounts to the volume fraction of free zone in the whole computing region. From the sketch shown in Fig. 4, we define $\delta = L_f/L_a$, and the volume fraction of free zone in all computing regions becomes δ^3 for the three-dimension problem. When $\delta = 0$, it reverts back to the original Berendsen barostat.

In order to verify the effectiveness of the partial Berendsen barostat, we first apply it to the single-component situation with varied volume fractions ($\delta = 0 \sim 1.0$) and the initial size (particle number is 108 000) of the computation region is kept the same for different cases. The steady system pressure is calculated and the pressure deviation from the desired pressure as well as the system temperature deviation are given in Fig. 5. It shows that there is a critical δ , which is 0.6 for DPD and 0.8 for MDPD in the current situation. Correspondingly, the dimensionless minimum thickness of the rescaling zone with respect to the side length of the free zone can be obtained as 0.333 in DPD and 0.125 in MDPD. For cases with δ beyond the critical value, the partial Berendsen barostat becomes invalid with unacceptable pressure deviation, and also the intrinsic thermostat of (M)DPD does not work. This critical δ has a dependence on the simulation size. In the following, the same simulation size is chosen and hence same δ is applied. We define a new variable to measure the system temperature deviation, which



FIG. 4. Structure of the partial Berendsen barostat in one direction. The gray part (top and bottom) is the rescaling zone, and the scattered part is the free zone.

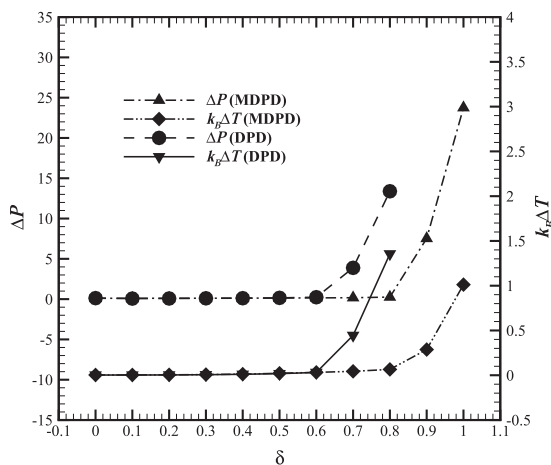


FIG. 5. Pressure and temperature fluctuations, when the (M)DPD fluid is kept in constant pressure condition by the partial Berendsen barostat in the single-component system.

is the energy of the adiabatic heating

$$E_{ah} = k_B \int_0^{t_m} (T(t^*) - T_0) dt^*, \quad (17)$$

where T_0 is the ensemble temperature before $t = t_J$, and $T(t^*)$ is the temperature at $t = t^*$. Besides, the temperature reaches maximum or minimum value when $t^* = t_m$. The results are shown in Fig. 6, we can see that E_{ah} jumps to a much greater value when δ is larger than the critical value, which means that the thermostat cannot “consume” the energy to be potential energy of particles, and then this energy will be kept in the kinetic energy of particles, bringing more fluctuation to the particle velocity.

B. MDPD simulation in multi-component system by partial Berendsen barostat

We choose a multi-component system consisting of a spherical immiscible droplet or bubble (we prefer to name it bubble in the rest of the paper) and surrounding liquid. In our cases, the particle number is 108 000 in total, and the bubble

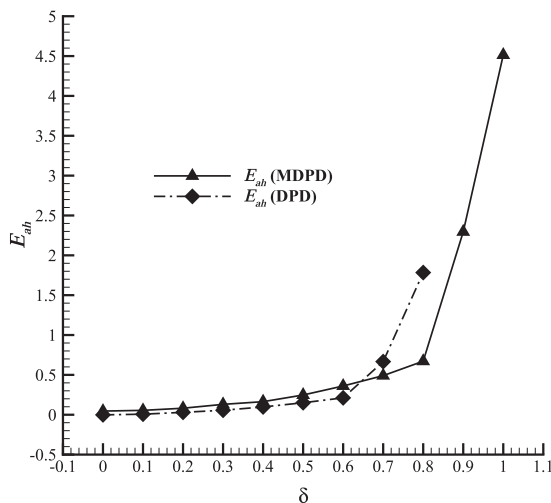


FIG. 6. Energy of the adiabatic heating in the single-component system with different δ .

TABLE IV. Simulation parameters of the bubble–liquid system.

	A_{ij}	B_{ij}	r_C	r_d
Bubble–bubble	-20	25	1.0	0.75
Liquid–liquid	-40	25	1.0	0.75
Bubble–liquid	20	/	1.0	/

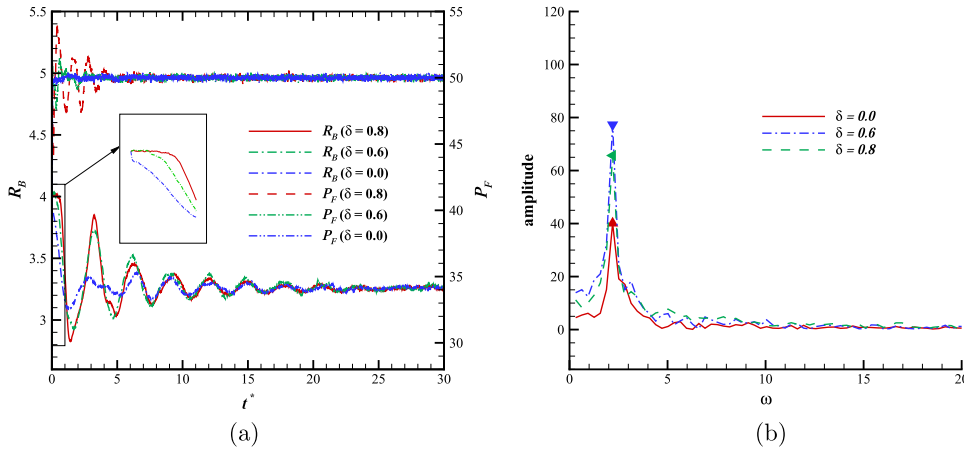
particle number is 848. The initial computation region size is $L = 26.5$, and the radius of the bubble is 3, resulting to the initial volume ratio of the bubble around 0.60% to the whole computation volume. The partial Berendsen barostat is applied to achieve a constant pressure condition of the surrounding fluid. Here, we give the same definition of δ by neglecting the bubble volume.

We build our simulation system by the MDPD method, and the force parameter and cutoff distance of interacting particles are shown in Table IV. The bubble radius R_B is obtained by the volume of fluid (VOF) method. The computation region is divided by many cubic lattices with the same side length equal to 1, and therefore the particle density of lattices is equal to the particle number. For the multi-component lattice, the volume of one single phase is directly proportional to the rate of particle number of this species to all particle numbers in this lattice. After summing up the single phase volume of all lattices, we can obtain the bubble volume. Using the sphere volume formula, the bubble radius is given by

$$R_B = \left(\frac{3}{4\pi} \sum_{i=1}^N \frac{n_{iB}}{n_{iP}} \right)^{\frac{1}{3}}, \quad (18)$$

where n_{iB} and n_{iP} are the number of bubble particles and all particles in i th lattices, respectively.

Particles in this multi-component system are first released to reach a stable state, and then the desired pressure of the barostat is increased which is similar as shown in Fig. 2(b). The effect of volume fraction (δ) is studied in the current multi-component system with $\delta = 0.0, 0.6, 0.8$ for three different cases. At initial state, the bubble pressure is $P_B = 5.016$, and the surrounding fluid pressure is $P_F = 0.184$ balanced with the surface tension. In the end, the system comes to a stable state with bubble pressure $P_B^* = 65.215$ and fluid pressure $P_F^* = 51.540$. We obtain the ensemble pressure by averaging last 5000 time steps for each phase, and we find that the final ensemble pressure of the fluid is very close to the desired pressure $P_0 = 50$ indicating that the partial Berendsen barostat still works well. However, the discrepancy happens in the early stage as shown in Fig. 7(a). It shows that the partial Berendsen barostat with $\delta = 0.6$ and 0.8 can capture the pressure fluctuation as well as bubble oscillation with sufficient large amplitude. Whereas the original Berendsen barostat ($\delta = 0.0$) inhibits both the pressure fluctuation and bubble oscillation, and therefore the dynamic behavior is missing. The radius variation of the bubble in the very early stage is shown in the subgraph; the bubble radius decreases quickly when $\delta = 0.0$ which is inconsistent with the other two cases. Therefore, the current partial Berendsen barostat can help us to capture the nonequilibrium phenomena and dynamic behaviors in the multi-component system properly.



The results in Fig. 7(a) show a constant frequency of bubble oscillation. Therefore, the dominant frequencies of bubble oscillation are extracted by the Fast Fourier Transform (FFT) from the curves of bubble radius, and the amplitude spectrum is shown in Fig. 7(b). The dominant frequencies are around $\omega_{FFT} = 2\pi f = 2.20$ for cases of different δ , while the amplitude of the $\delta = 0.0$ case deviates from the others. In order to validate the current simulation, the analytical solution of the natural frequency of bubble oscillation is employed for comparison.⁴⁴ This analytical solution is derived based on the classical Rayleigh–Plesset equation,⁴⁵ after a linearization approach. The natural frequency, ω_N , can be written as

$$\omega_N = \frac{1}{R_0} \sqrt{\frac{1}{\rho_l} (3kP_{g0} - \frac{2S}{R_0})}, \quad (19)$$

where P_{g0} and R_0 are the gas pressure and bubble radius in the equilibrium state, S is the surface tension, ρ_l is the surrounding liquid density, and k is the parameter in the EOS of gas. In the theory, the bubble pressure is built up as $P_B = P_v + P_g$, where P_v is the constant pressure in the bubble, and P_g is the gas pressure following the gas EOS as

$$P_g(R) = P_{g0} \left(\frac{R_0}{R} \right)^{3k}. \quad (20)$$

To be consistent, the parameter k is derived by a curve fitting with the current MDPD EOS, and $k = 7.79$ in the current work. The variables in Eq. (19) are obtained from our simulation. For the case of $\delta = 0.6$, we have $R_0 = 3.32$, $\rho_l = 6.89$, $P_{g0} = 24.25$, and $S = 30.61$, all are in DPD units. The resulted natural frequency is $\omega_N = 2.69$, close to our FFT result as $\omega_{FFT} = 2.20$. However, the error mainly comes from two parts. First, the analytical solution is based on a linear equation, without considering the nonlinear effect. Second, our bubble model in the MDPD simulation has a finite mass ratio to the surrounding liquid, while this ratio is close to zero in the original theory of Rayleigh–Plesset equation. The inertial effect may take place in our MDPD simulation.

C. Applications of the partial Berendsen barostat in multi-component system

In this subsection, emphasis is put on two typical applications of the partial Berendsen barostat in the multi-component

system and NEDP. The development of the current partial Berendsen barostat model is motivated from studies on micro- and nanobubbles. For example, growth and collapse of microbubble are the key phenomena in cavitation,⁴⁶ which can significantly affect the hydrodynamic performance of a propeller. Single bubble-vesicle interactions can be applied in drug delivery and cell manipulation.⁴⁷ We are aiming to show the feasibility of the current partial Berendsen barostat in these applications, and therefore to investigate the physical behavior of this multi-component system and their NEDP.

1. Vapor–liquid coexistence system under square wave pressure condition

The vapor–liquid coexistence system under square wave pressure is first studied. Unlike the multi-component model in Section IV B, here we use the MDPD particle to represent the liquid phase, whereas the vapor phase is identified by the vacuum region. This is a common way to build the vapor–liquid coexistence system, which has been investigated by Warren¹¹ and Arienti *et al.*⁴⁸ in MDPD, Okumura and Ito⁴⁹ in MD. Besides, Fu *et al.* also built the same vapor–liquid system in MD and CG MARTINI methods to study the interaction of the collapsing bubble and lipid layer membrane.⁴³

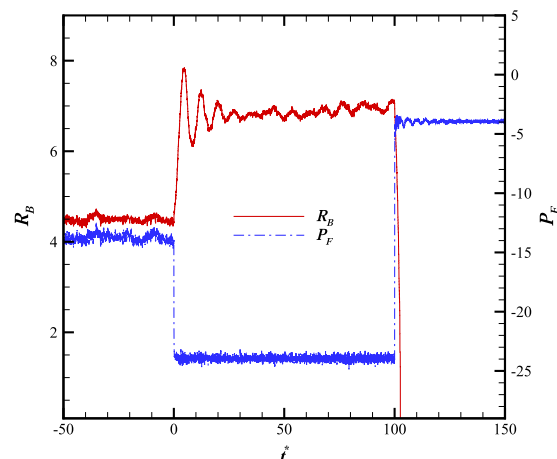


FIG. 8. Vapor-liquid coexistence system under square wave pressure condition with $\delta = 0.6$, and the square pressure wave is given by Eq. (15), where $P_0 = P(t^* = 0)$, $P_a = 10$, and $f = 5 \times 10^{-3}$.

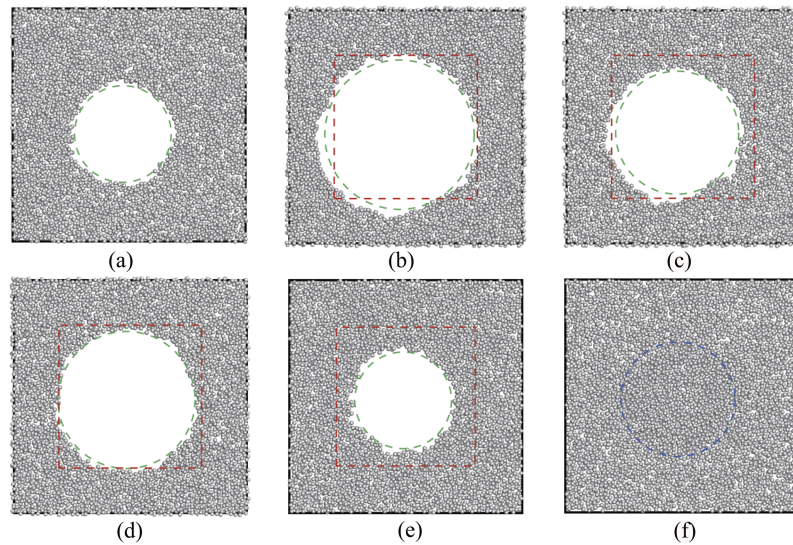


FIG. 9. Detailed slices of particle distribution at different instances, (a) $t^* = 0.0$; (b) $t^* = 5.0$; (c) $t^* = 10.0$; (d) $t^* = 100.0$; (e) $t^* = 101.5$; (f) $t^* = 103.0$. The dashed dot red frame represents the free zone boundary; the dashed green circle is a reference circle.

Because of the vacuum bubble region, the particle number is reduced to 107 336, while the initial computation region is of the same size in Sec. IV A. We apply the square wave pressure condition (similar as Fig. 3) with one period time to stimulate the bubble growing and collapsing process. Because there are no bubble particles in this model, a different calculation of bubble radius from Eq. (18) is derived as follows:

$$R_B = \left(\frac{3}{4\pi} N_v \right)^{\frac{1}{3}}, \quad (21)$$

where N_v is the number of vacuum lattices. In this way, the bubble radius will be accurate when the bubble size is large enough, but it will lead to vanish instantly when the bubble radius is smaller than $1/\sqrt{2}$. The histories of bubble radius and system pressure are shown in Fig. 8. We can see that the bubble grows with fluctuation corresponding to the pressure reduction and it collapses quickly once the pressure recovers. It is worthy to mention that the system pressure is negative due to balance of the zero internal pressure (bubble pressure) and the non-zero surface tension. The detailed slices of particle distribution are shown in Fig. 9 at different times. The dashed dot red frame in certain subfigures represents the free zone boundary. In Figs. 9(a) and 9(d), the vapor–liquid system is in a balanced and stable situation according to Fig. 8, and the bubble area is in the free zone region. Concerning the subfigures in Figs. 9(b), 9(c), and 9(e), a part of the bubble area is out of the free zone, and the bubble is not spherical compared with the dashed green reference circle, since particles out of the free zone are influenced by the rescaling process of the Berendsen barostat resulting in an unphysical shape of the interface. In addition, the blue circle in the last subfigure indicates the high density region caused by the inertial effect of bubble collapse. In conclusion, the proposed partial Berendsen barostat can be applied in the multi-component system with (M)DPD simulation for controlling pressure, and meanwhile, a large free zone region may help to retain the correct physical behaviors around the interface, and also to capture dynamic phenomena properly.

2. Multi-component system under harmonic wave pressure condition

Bubble oscillation under an ultrasound system could be a key for many kinds of biophysical and medical problems. Ultrasound is capable of increasing the permeability of cell membranes to drugs, allowing even poorly bioavailable drugs to be delivered with sufficient quantity, and the bubble (gaseous phase) collapse will lead to the enhancement of bilayer permeability.⁴³ Moreover, the oscillating bubbles can control the vesicle defaturation and lysis.⁴⁷ Another popular application is ultrasound imaging, where microbubble ultrasound contrast agents and cavitation microbubbles play a significant role in diagnostic applications.⁵⁰ We use the harmonic pressure condition to mimic the flow under the ultrasonic waves, and then the bubble will oscillate with the harmonic pressure.

The same multi-component system in Sec. IV A is chosen under the harmonic pressure to study NEDP by our partial barostat ($\delta = 0.6$). The bubble radius obtained is by Eq. (18).

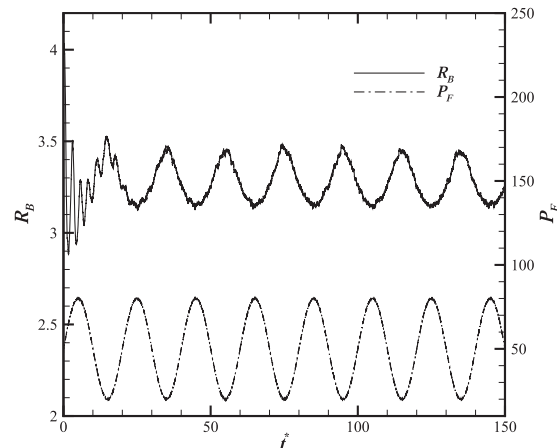


FIG. 10. MDPD multi-component system under harmonic pressure condition by the partial Berendsen barostat. The harmonic pressure wave is given by Eq. (16), where $P_0 = 50$, $P_a = 30$, and $f = 0.5$.

The results are shown in Fig. 10; the bubble radius oscillates following the pressure wave as we desired. Meanwhile, some large fluctuations of bubble radius are also captured in the early period when the desired system pressure changes drastically.

V. CONCLUSION

Constant pressure condition and controlling of system pressure are common in numerical simulation and experimental studies. The well-known Berendsen barostat is applied in both standard dissipative particle dynamics (DPD) and many-body dissipative particle dynamics (MDPD) simulation. The original Berendsen barostat works well in the (M)DPD simulation of the single-component system under constant pressure condition and nonequilibrium dynamic process, e.g., system pressure with square wave and harmonic wave shapes.

The partial Berendsen barostat is proposed to study the multi-component system in (M)DPD simulation. Only certain particles in the part region of the computational domain are involved in the rescaling process of the Berendsen barostat to achieve the desired pressure. The rest of the part forms the free zone region, in which the interface shape and nonequilibrium dynamic behavior between different phases can be captured properly. Several applications of the current partial Berendsen barostat are presented. An immiscible bubble in the second fluid under constant pressure condition is first studied, and the oscillation of bubble radius and fluctuation of system pressure can be obtained in the current simulation. For the application in ultrasound imaging and drug delivery, prototype models for bubble growing and collapsing under square wave of pressure and bubble oscillation under harmonic pressure wave are also reported in our simulation. It shows that the partial Berendsen barostat could be a good candidate for the study on single or few droplets/bubbles under certain pressure control in nonequilibrium dynamics. On the other hand, the study on many droplets/bubbles is also important and relevant in applications. Some improvement in the current partial Berendsen barostat model could be made in the future. For example, Maheshwari *et al.*⁵¹ used the so-called “semi-isotropic pressure control” approach in MD simulation of nanobubbles, in which the rescaling process in the barostat is only applied in one direction. Following this idea, the partial Berendsen barostat can be improved by adding the rescaling zone only on the top and bottom, with periodic boundary conditions on the left and right, and front and back of the free zone.

ACKNOWLEDGMENTS

The authors thank the reviewers for their valuable comments and suggestions. The authors are also grateful for the support of the National Natural Science Foundation of China (Grant Nos. 11402230, 91634103, and 11332009).

- ¹Z. G. Mills, W. Mao, and A. Alexeev, *Trends Biotechnol.* **31**, 426 (2013).
- ²S. Trofimov, E. Nies, and M. Michels, *J. Chem. Phys.* **123**, 144102 (2005).
- ³J. Koelman and P. Hoogerbrugge, *Europhys. Lett.* **21**, 363 (1993).
- ⁴E. Boek, P. V. Coveney, H. Lekkerkerker, and P. van der Schoot, *Phys. Rev. E* **55**, 3124 (1997).
- ⁵Y. Kong, C. Manke, W. Madden, and A. Schlijper, *Int. J. Thermophys.* **15**, 1093 (1994).
- ⁶A. Schlijper, P. Hoogerbrugge, and C. Manke, *J. Rheol.* **39**, 567 (1995).
- ⁷Y. Kong, C. Manke, W. Madden, and A. Schlijper, *J. Chem. Phys.* **107**, 592 (1997).
- ⁸N. Spenley, *Europhys. Lett.* **49**, 534 (2000).
- ⁹W. Jiang, J. Huang, Y. Wang, and M. Laradji, *J. Chem. Phys.* **126**, 044901 (2007).
- ¹⁰D. Pan, J. Hu, and X. Shao, *Mol. Simul.* **42**, 328 (2016).
- ¹¹P. Warren, *Phys. Rev. E* **68**, 066702 (2003).
- ¹²D. Pan, N. Phan-Thien, and B. C. Khoo, *J. Non-Newtonian Fluid Mech.* **212**, 63 (2014).
- ¹³D. Pan, N. Phan-Thien, and B. C. Khoo, *Mol. Simul.* **41**, 1166 (2015).
- ¹⁴D.-y. Pan, Y.-q. Lin, L.-x. Zhang, and X.-m. Shao, *J. Hydronaut.* **28**, 702 (2016).
- ¹⁵S. Jury, P. Bladon, M. Cates, S. Krishna, M. Hagen, N. Ruddock, and P. Warren, *Phys. Chem. Chem. Phys.* **1**, 2051 (1999).
- ¹⁶R. D. Groot, *Langmuir* **16**, 7493 (2000).
- ¹⁷R. D. Groot, *J. Chem. Phys.* **118**, 11265 (2003).
- ¹⁸L. Rekvig, M. Kranenburg, J. Vreede, B. Hafskjold, and B. Smit, *Langmuir* **19**, 8195 (2003).
- ¹⁹M. Venturoli and B. Smit, *PhysChemComm* **2**, 45 (1999).
- ²⁰R. D. Groot and K. Rabone, *Biophys. J.* **81**, 725 (2001).
- ²¹K. Yang and Y.-Q. Ma, *Nat. Nanotechnol.* **5**, 579 (2010).
- ²²M. Dutt, O. Kuksenko, S. R. Little, and A. C. Balazs, *Nanoscale* **3**, 240 (2011).
- ²³Y. Li, X. Li, Z. Li, and H. Gao, *Nanoscale* **4**, 3768 (2012).
- ²⁴H. Djohari and E. E. Dormidontova, *Biomacromolecules* **10**, 3089 (2009).
- ²⁵M. D. Tomasini and M. S. Tomassone, *Chem. Eng. Sci.* **71**, 400 (2012).
- ²⁶K. Patterson, M. Lisal, and C. M. Colina, *Fluid Phase Equilib.* **302**, 48 (2011).
- ²⁷H. Masoud and A. Alexeev, *ACS Nano* **6**, 212 (2011).
- ²⁸M. Delcea, H. Möhwald, and A. G. Skirtach, *Adv. Drug Delivery Rev.* **63**, 730 (2011).
- ²⁹H. J. Berendsen, J. P. M. Postma, W. F. van Gunsteren, A. DiNola, and J. Haak, *J. Chem. Phys.* **81**, 3684 (1984).
- ³⁰M. Lísal, J. K. Brennan, and J. B. Avalos, *J. Chem. Phys.* **135**, 204105 (2011).
- ³¹A. F. Jakobsen, *J. Chem. Phys.* **122**, 124901 (2005).
- ³²M. A. Seaton, R. L. Anderson, S. Metz, and W. Smith, *Mol. Simul.* **39**, 796 (2013).
- ³³M. Atashafrooz and N. Mehdipour, *J. Chem. Eng. Data* **61**, 3659 (2016).
- ³⁴P. Hoogerbrugge and J. Koelman, *Europhys. Lett.* **19**, 155 (1992).
- ³⁵I. Pagonabarraga and D. Frenkel, *J. Chem. Phys.* **115**, 5015 (2001).
- ³⁶S. Trofimov, E. Nies, and M. Michels, *J. Chem. Phys.* **117**, 9383 (2002).
- ³⁷P. Espanol and P. Warren, *Europhys. Lett.* **30**, 191 (1995).
- ³⁸M. P. Allen and D. J. Tildesley, *Computer Simulation of Liquids* (Oxford University Press, 1989).
- ³⁹R. D. Groot and P. B. Warren, *J. Chem. Phys.* **107**, 4423 (1997).
- ⁴⁰D. Pan, N. Phan-Thien, N. Mai-Duy, and B. C. Khoo, *J. Comput. Phys.* **242**, 196 (2013).
- ⁴¹J. Irving and J. G. Kirkwood, *J. Chem. Phys.* **18**, 817 (1950).
- ⁴²W. K. Den Otter and J. H. R. Clarke, *Int. J. Mod. Phys. C* **11**, 1179 (2000).
- ⁴³H. Fu, J. Comer, W. Cai, and C. Chipot, *J. Phys. Chem. Lett.* **6**, 413 (2015).
- ⁴⁴C. E. Brennen, *Cavitation and Bubble Dynamics* (Cambridge University Press, 2013).
- ⁴⁵M. S. Plesset and A. Prosperetti, *Annu. Rev. Fluid Mech.* **9**, 145 (1977).
- ⁴⁶K. A. Mørch, *Interface Focus* **5**, 20150006 (2015).
- ⁴⁷P. Marmottant and S. Hilgenfeldt, *Nature* **423**, 153 (2003).
- ⁴⁸M. Arienti, W. Pan, X. Li, and G. Karniadakis, *J. Chem. Phys.* **134**, 204114 (2011).
- ⁴⁹H. Okumura and N. Ito, *Phys. Rev. E* **67**, 045301 (2003).
- ⁵⁰E. Stride and C. Coussios, *Proc. Inst. Mech. Eng., Part H* **224**, 171 (2010).
- ⁵¹S. Maheshwari, M. van der Hoef, X. Zhang, and D. Lohse, *Langmuir* **32**, 11116 (2016).